JACS
JOURNAL OF THE AMERICAN CHEMICAL SOCIETY

Article

pubs.acs.org/JACS

Atomic-Scale Recognition of Surface Structure and Intercalation Mechanism of Ti_3C_2X

Xuefeng Wang,[†] Xi Shen,[‡] Yurui Gao,[†] Zhaoxiang Wang,*[,†] Richeng Yu,*[,‡] and Liquan Chen[†]

[†]Key Laboratory for Renewable Energy, Chinese Academy of Sciences, Beijing Key Laboratory for New Energy Materials and Devices, Beijing National Laboratory for Condensed Matter Physics, Institute of Physics, Chinese Academy of Sciences, P.O. Box 603, Beijing 100190, China

[‡]Laboratory for Advanced Materials & Electron Microscopy, Beijing National Laboratory for Condensed Matter Physics, Institute of Physics, Chinese Academy of Sciences, P.O. Box 603, Beijing 100190, China

Supporting Information

ABSTRACT: MXenes represent a large family of functionalized two-dimensional (2D) transition-metal carbides and carbonitrides. However, most of the understanding on their unique structures and applications stops at the theoretical suggestion and lack of experimental support. Herein, the surface structure and intercalation chemistry of Ti_3C_2X are clarified at the atomic scale by aberration-corrected scanning transmission electron microscope (STEM) and density functional theory (DFT) calculations. The STEM studies show that the functional groups (e.g., OH^-, F^-, O^-) and the intercalated sodium (Na) ions prefer to stay on the top sites of the centro-Ti atoms and the C atoms of the Ti_3C_2 monolayer, respectively. Double Na-atomic layers are found within the Ti_3C_2X interlayer upon extensive Na intercalation via two-phase transition and solid-solution reactions. In addition, aluminum (Al)-ion intercalation leads to horizontal sliding of the Ti_3C_2X monolayer. On the basis of these observations, the previous monolayer surface model of Ti_3C_2X is modified. DFT calculations using the new modeling help to understand more about their physical and chemical properties. These findings enrich the understanding of the MXenes and shed light on future material design and applications. Moreover, the Ti_3C_2X exhibits prominent rate performance and long-term cycling stability as an anode material for Na-ion batteries.

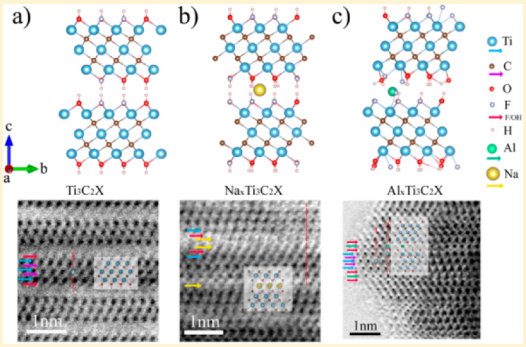

INTRODUCTION

Two-dimensional (2D) materials have been extensively exploited and have shown great potential in various applications due to their unique physical structures and chemical properties. Attention has been further gained since the discovery of graphene in 2004,[1] which is composed of single layers of sp^2-hybridized carbon atoms and exhibits outstanding electronic properties. Other 2D materials have been obtained from solids with weak interlayer interactions, such as boron nitride,[2] metal chalcogenides,[3,4] oxides,[5,6] and hydroxides.[7] Owing to their single- or few-layer characteristics, these 2D materials show many advantages in a wide range of applications.[8−14]

Recently, a new family of 2D materials, called MXenes,[15] has been fabricated from early transition metal carbides and/or carbonitrides known as MAX phases[16] with strong interlayer mixed covalent or metallic ionic bondings[17] by etching off the A atoms. There are more than 60 MAX phases, some of which have been successfully exfoliated to MXenes, including Ti_3C_2, Nb_2C, V_2C, $(Ti_{0.5}Nb_{0.5})_2C$, Ti_3CN, etc.[15,18−20] These MXene nanosheets have rich surface chemistries and high electronic conductivities and exhibit prominent performance in catalysis chemistry and energy storage systems.[18,21−24] However, most of the understanding of MXenes stops at theoretical predictions, and experimental recognition has not been sufficiently made.

Surface structure is definitely crucial for the distinctive properties of the MXenes as many functional groups (OH^-, F^-, O^-) are terminated on the surface after hydrogen fluoride (HF) treatment for removing the A atoms. Theoretical calculations show that the thermodynamic stability, electronic properties, and even the intercalation mechanisms of the MXenes are closely related with their surface terminations.[15,25−29] For example, the Ti_3C_2 monolayer is metallic, but its fluorinated or hydroxylated derivatives are narrow-gap semiconductors.[25] Moreover, the surface functional groups are sensitive to the adsorption of metal ions, such as Li, Na, K, Ca, Mg, and Al[26,28−30] and further affect the intercalation chemistry as well as their storage capacity and operation potential when the MXenes are applied in rechargeable batteries. However, these predictions are only based on theoretical modeling of surface termination on perfect monolayer and lack of experimental support. Further, in contrast to the current calculations based on monolayer MXenes, most of the as-prepared MXenes are stacked and have interlayer interactions, as other 2D materials do.

Herein, the surface structure of Ti_3C_2X (X = OH, F, and O) is disclosed at the atomic scale as well as their derivate structures

Received: December 17, 2014
Published: February 6, 2015

DOI: 10.1021/ja512820k
J. Am. Chem. Soc. 2015, 137, 2715−2721

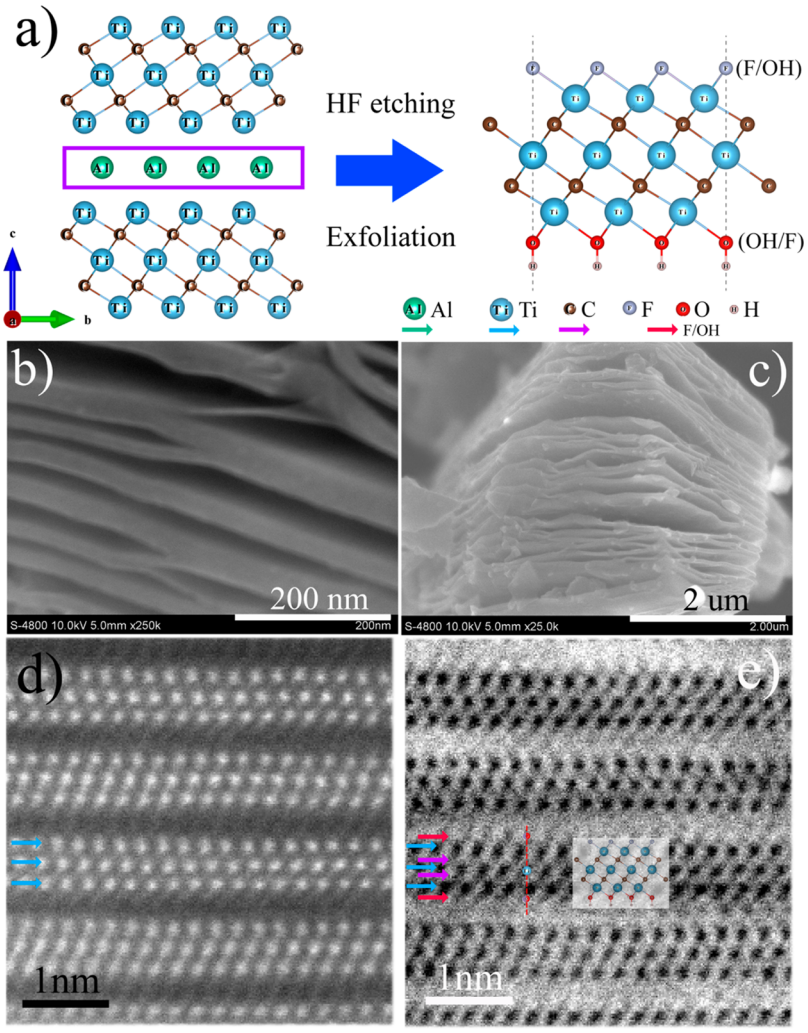

Figure 1. Schematic description of the synthesis and structure of Ti_3C_2X (a), SEM (b, c), HAADF (d), and ABF (e) images of Ti_3C_2X observed along the *a*/*b* axis. Two C atomic layers (labeled with purple arrows) interleave into three Ti-atomic layers (labeled with blue arrows) with a sequence of Ti(s)−C−Ti(c)−C−Ti(s), forming an edge-shared TiC_6 octahedral stacking. The functional groups such as O and/or F atoms (labeled with red arrows) prefer to stay on top of the Ti(c) atoms, instead of the topmost sites of the C atoms on both sides of the Ti_3C_2 layer.

upon intercalation of ions such as Na and Al. Combined with experimental observations at the atomic scale, the surface model of Ti_3C_2X and other calculations are modified or improved. Our findings deepen the understanding on both the structure and intercalation chemistry of MXenes and also provide a useful guidance to theoretical modeling.

RESULTS AND DISCUSSION

Surface Structure of Ti_3C_2X. Ti_3C_2X (X = OH, F, and O) nanosheets with expanded layers were obtained (Figure 1a for schematic synthesis process) by immersing the layer-structured Ti_3AlC_2 (Supporting Information Figure S1 for its morphology) in HF solution for 12 h to remove the Al atoms. Scanning electron microscopy (SEM) images (Figure 1b,c) show multilayer-stacked Ti_3C_2X nanosheets, ranging from a few nanometers to ca. 45 nm in thickness. Powder X-ray diffraction (XRD) results (Supporting Information Figure S2a) indicate that Ti_3C_2X has larger *c* values (ca. 19.9 Å) than Ti_3AlC_2 (ca. 18.5 Å). The interactions between the adsorbed functional groups such as OH^-, F^-, O^- and the Ti_3C_2 monolayer are found to be chemical such as Ti−O (Ti $2p_{3/2}$; 456.3 eV), Ti−F (Ti $2p_{3/2}$; 459.3 eV) by X-ray photoelectron spectroscopy (XPS) (Supporting Information Figure S2b). The content of F and O was determined to be ca. 20.15 and 10.36 at. %, respectively. Moreover, red shifting of about 0.6 eV was observed for the Ti−C bonding (Ti $2p_{3/2}$; 454.5 eV in Ti_3AlC_2, 455.1 eV in Ti_3C_2X; Supporting Information Figure S2c,d), suggesting that both the Ti and C atoms are oxidized to some extent after Al removal.

Advanced aberration-corrected scanning transmission electron microscopy (STEM) was employed along the *a*/*b* axis of Ti_3C_2X to reveal its surface structure. The high-angle annular dark-field (HAADF) image (Figure 1d) shows that three Ti atomic layers (labeled with blue arrows) construct the skeleton of the Ti_3C_2X monolayer and stack into nanosheets following a sequence of ABAB, where A and B stand for the adjacent two Ti_3C_2 monolayers.[31] Its average interlayer spacing is measured to be about 0.98 nm, consistent with the XRD results (Supporting Information Figure S2a). As it is difficult to recognize light atoms such as C, O, and F in the HAADF images, annular bright-field (ABF) images are combined with the HAADF to figure out these difficulties. Figure 1e shows that two C atomic layers (labeled with purple arrows) interleave into three Ti-atomic layers with a sequence of Ti(s)−C−Ti(c)−C−Ti(s) (Ti(s) stands for the Ti near the surface and Ti(c) for the central Ti), forming an

DOI: 10.1021/ja512820k
J. Am. Chem. Soc. 2015, 137, 2715−2721

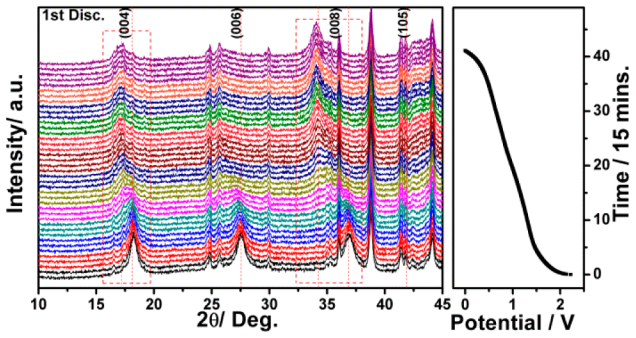

Figure 2. In situ XRD patterns of Ti_3C_2X during electrochemical intercalation of the Na ions. The XRD patterns indicate that Na ions are intercalated into Ti_3C_2X reversibly via two-phase transition and solid-solution reactions.

edge-shared TiC_6 octahedral stacking (Figure 1a). It seems that the O and/or F atoms prefer to stay over the vacant sites between the three neighboring C atoms, namely the position on top of the Ti(c) atoms, instead of the topmost sites of the C atoms on both sides of the Ti_3C_2 layer. The vertical distance from the O/F layer (labeled with red arrows just out of the Ti(s) layers) to the Ti(c) layer is about 0.35 nm. These observations are in line with the previous calculations based on monolayer modeling.[25,26] However, as multilayer stacking is often found in reality, interlayer interactions such as the van der Waals force and/or hydrogen bonding should therefore be taken into account. Furthermore, the functional groups are believed to be randomly distributed rather than in a special one such as alternate O- and F atomic layers, for example. This is verified with the irregular content trends of O/F atoms detected by energy-dispersive spectroscopy

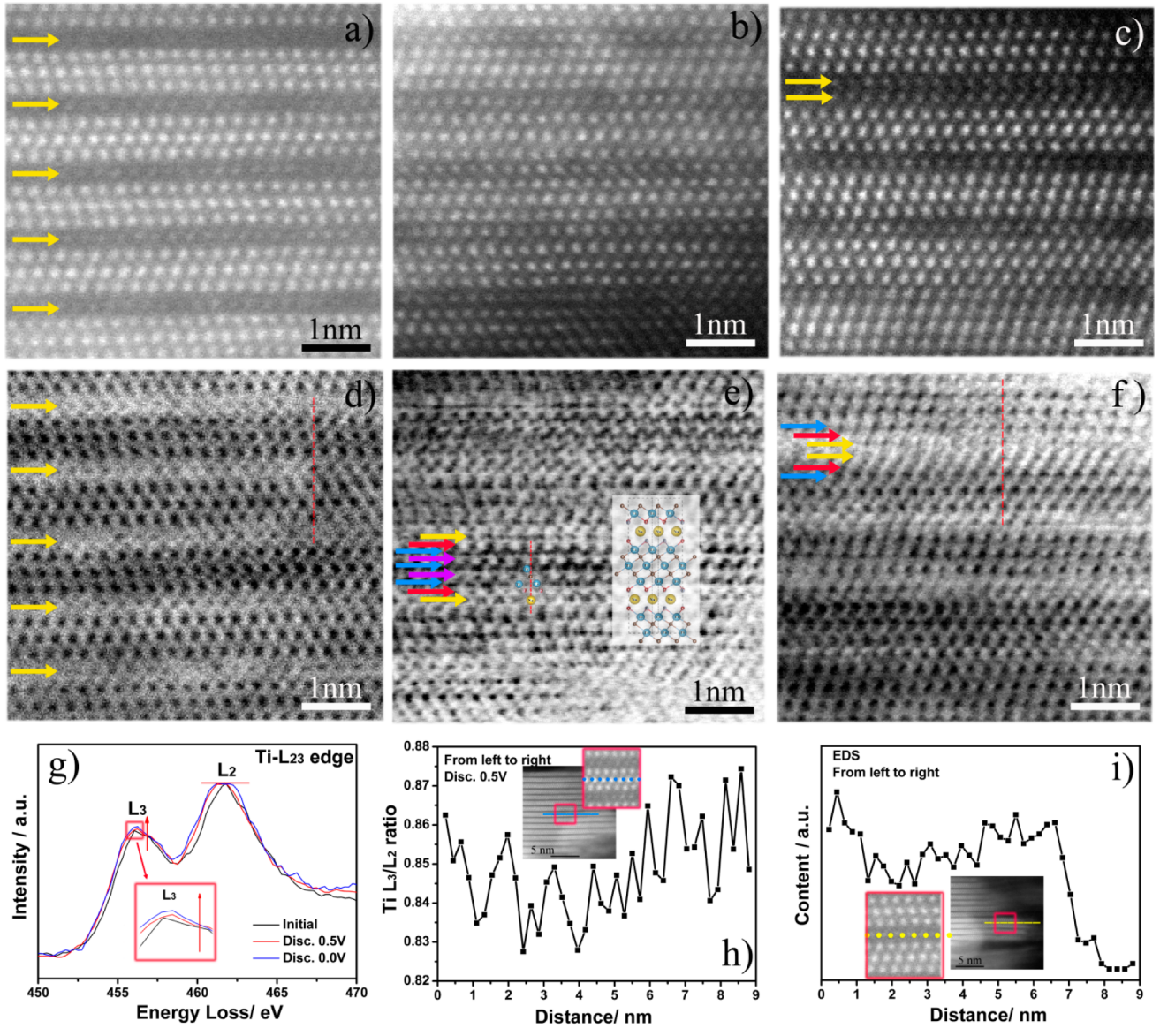

Figure 3. HAADF (a–c) images, ABF (d–f) images, EELS spectra (g), the changes of Ti L_3/L_2 intensity ratio (h), and Na content (i) from left to right (i.e., from bulk to surface) of Ti_3C_2X electrodes upon Na intercalation with cutoff potential of 0.5 V (a, d, h, i) and 0.0 V (b, c, e, f). The insets in parts h and i are the HAADF images of the selected area for EELS and EDS. The Na ions are intercalated into Ti_3C_2X from the surface, partially (a and d) or fully (b, c, e, and f) occupy the interlayers and stay on top of the C atoms rather than on top of the Ti(s) or Ti(c) atoms in the Ti_3C_2X layer. Moreover, double Na-atomic layers are observed in one interlayer of the fully intercalated sample (c; labeled with double yellow arrows).

DOI: 10.1021/ja512820k
J. Am. Chem. Soc. 2015, 137, 2715–2721

(EDS) (Supporting Information Figure S3). In light of these observations, the previous monolayer modeling needs to be modified. The results of density functional theory (DFT) calculations based on the modified model are shown and discussed later in this Article (Figure 6).

Sodium Intercalation in Ti_3C_2X. Intercalation chemistry is one of the most important bases for energy conversion and storage[32,33] as well as two-dimensional nanosheets preparation.[34,35] A variety of cations and molecules, including Na^+, K^+, NH_4^+, Mg^{2+}, Al^{3+}, hydrazine, and urea, have been intercalated in MXenes by chemical or electrochemical methods.[22,24] However, their intercalation mechanisms remain unclear. To address this question, STEM and in situ XRD are combined to illustrate the structural evolution and atomic occupation upon Na-ion intercalation in Ti_3C_2X.

In situ XRD (Figure 2) was performed on a Ti_3C_2X/Na cell cycled between 0.01 and 2.50 V at a current density of 10 mA g^{-1}. Clearly, phase transition occurs from Ti_3C_2X to $NaTi_3C_2X$ during Na-ion intercalation as the diffraction peaks of Ti_3C_2X gradually fade while some new peaks appear and grow at the low diffraction angle side. As intercalation goes further, only $NaTi_3C_2X$ phase can be detected and its (004) and (008) diffraction peaks shift toward the lower angles continuously, suggesting that a solid solution reaction occurs. These structural changes are reversible as an inverse evolution process is observed in the subsequent deintercalation (Supporting Information Figure S4). In addition, as these two phases share the same (105) diffraction peak and only the (00l) (l = 2, 4, 6, 8, etc.) diffraction peaks vary, the intercalated Na ions are supposed to stay in the interlayers of Ti_3C_2X.

The structural changes and atomic occupation upon Na ion intercalation are recognized at the atomic scale by STEM. The intercalation process of the Na ions (discharge) in the Ti_3C_2X can be controlled by tuning the cutoff discharge potential in a galvanostatic mode. Electrodes with partial intercalation (cutoff at 0.5 V) and full intercalation (cutoff at 0.0 V) are explored (Figure 3). These images clearly show that the Na ions are intercalated into the interlayers of Ti_3C_2X, labeled with yellow arrows. These intercalated Na ions can partially (Figure 3a,d) or fully (Figure 3b,c,e,f) occupy the interlayers in the samples, as indicated by the dim and distinct white Na atoms in the HAADF images, respectively. The gradually darkening interlayer points from left to right (that is, from the bulk to the surface of the sample) in the ABF images (Figure 3d), suggest that the Na ions are intercalated at the surface and then diffused into the bulk.

The above points are confirmed with the electron energy loss spectroscopy (EELS; Figure 3h) and EDS (Figure 3i). Two edges of Ti are observed in the EELS spectrum (Figure 3g), known as L_2 (456.4 eV), L_3 (461.7 eV), and their intensity ratio L_3/L_2 is related with the fine structure as well as the chemical states of Ti_3C_2X.[36,37] The intercalated Na ions donate electrons to Ti_3C_2X, resulting in the reduction of the Ti atoms and the increase of the L_3/L_2 intensity ratio (Figure 3g) though these changes are not obvious. Therefore, in the case of the partially intercalated sample, the gradually increased L_3/L_2 ratio in EELS spectra (Figure 3h) and Na content in EDS spectra (Figure 3i) from left to right further manifest that the intercalation starts at the surface.

The position and coverage of the intercalated Na ions are another two important issues to be concerned. Careful checking of the Na position in the interlayer (highlighted with red lines in Figure 3d–f) finds that the intercalated Na ions prefer to stay on top of the C atoms rather than on top of the Ti(s) or Ti(c) atoms in the Ti_3C_2X layer, in accordance with previous predictions.[25−28] On the other hand, the functional groups slightly shift from their original sites (on top of the Ti(c) atoms). The vertical distances from the O/F and Na atomic layer to the Ti(c) atomic layer are about 0.31 and 0.44 nm, respectively; the former is smaller than the original value (0.35 nm). Further, the distance between the O/F and the Ti(s) atoms is smaller than that between the O/F and the Na atoms (~0.12 vs ~0.18 nm), indicating that functional groups (e.g., O/F) incline to bond with the Ti(s) atoms instead of the Na atoms. Moreover, double Na-atomic layers are observed in one interlayer of the fully intercalated sample (Figure 3c; labeled with double yellow arrows). Recent reports[26,28] predicted that double Li and Na layers can be formed in a monolayer of Ti_3C_2X. That is true for this case. The double Na atomic layers share the same site (on top of the C atoms) and are about 0.23 nm apart from each other. Combined with the above in situ XRD results, this process is believed to have taken place at the final intercalation, that is, during the solid solution reaction.

The intercalation of the hypervalent metal ions (e.g., Al^{3+}) into Ti_3C_2X is supposed to be different from that of the alkali metals. A previous study showed that less than $^2/_3$ of a monolayer of the Ti_3C_2X can be covered (to have species adsorbed on) with Al

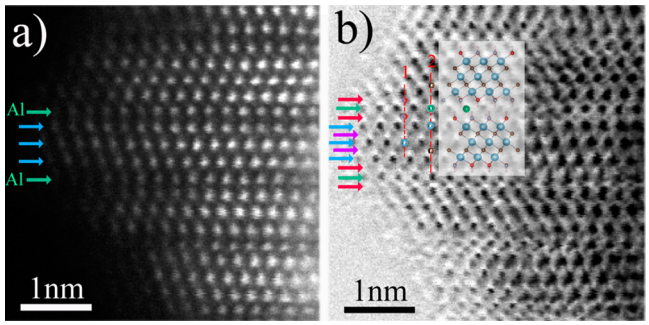

Figure 4. HAADF (a) and ABF (b) images of Ti_3C_2X upon Al intercalation. Intercalation of the Al ions (labeled with green arrows) induces horizontal sliding of the Ti_3C_2X monolayer.

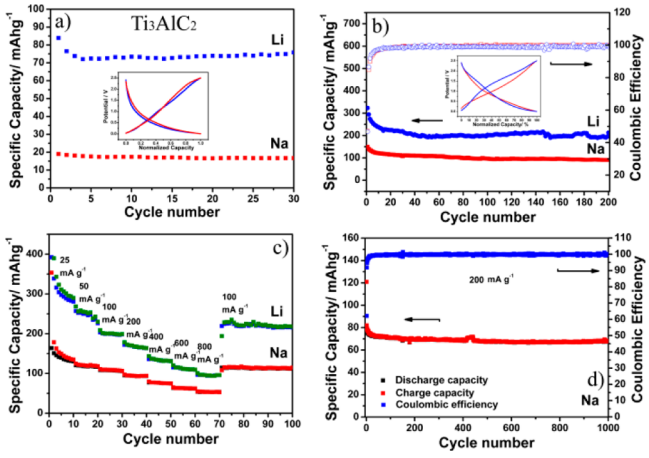

Figure 5. Electrochemical performances of Ti_3AlC_2 (a) and Ti_3C_2X (b–d) for LIB and NIB. (b) Cycling performance at 50 mA g^{-1}, (c) rate performance of Ti_3C_2X for LIB and NIB. (d) Long-term cycling performance of Ti_3C_2X at 200 mA g^{-1} for NIB. The insets in a and b are the potential profiles of the selected cycles. The Ti_3C_2X nanosheets exhibit excellent rate performance (c) and long-term cycling stability (d). The slight fluctuation of specific capacity of Ti_3C_2X is due to the subtle changes of the test atmosphere, such as temperature.

DOI: 10.1021/ja512820k
J. Am. Chem. Soc. 2015, 137, 2715−2721

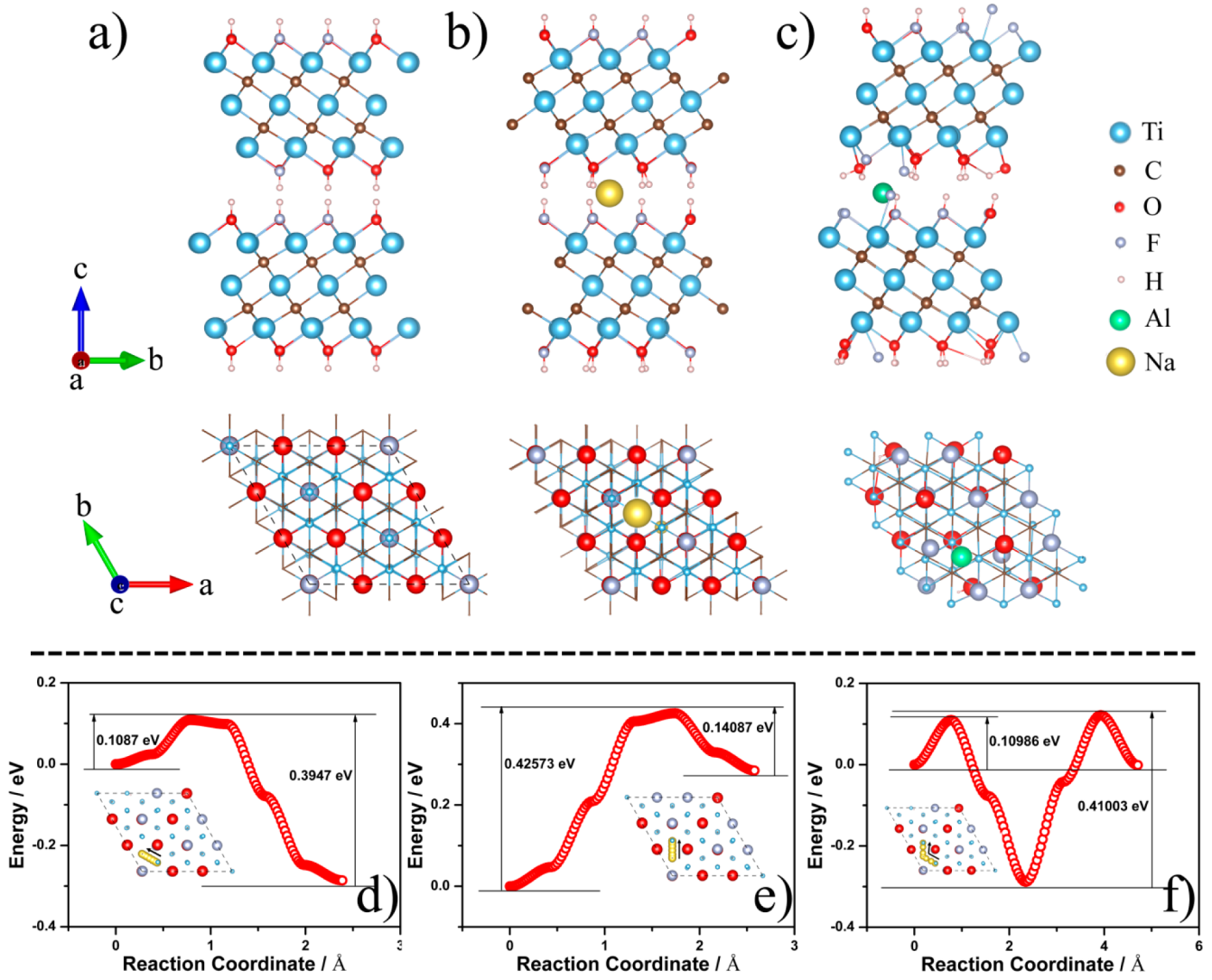

Figure 6. Optimized geometries of Ti_3C_2X (a), $Na_xTi_3C_2X$ (b), $Al_xTi_3C_2X$ (c) from side and top view; the diffusion barrier profiles of Na on Ti_3C_2X via the predesigned pathways (d–f). Their insets show the possible migration paths for Na diffusion in Ti_3C_2X from top view. The DFT calculations were performed with a modified model based on our experimental results and indicate that the Na ions can easily diffuse in Ti_3C_2X.

atoms.[28] However, this is indistinguishable in the STEM images because a spot in the STEM images stands for a column of atoms. In this case, it seems that the Al ions can occupy the full interlayer of Ti_3C_2X (Figure 4a,b). Furthermore, intercalation of the Al ions induces horizontal sliding of the Ti_3C_2X monolayer. Therefore, the Al ions are located at the top sites of C of one Ti_3C_2X layer and close to the top sites of Ti(s) of the other layer. The vertical distances from the Al atomic layer (labeled with green arrows) to the Ti(s), C, and Ti(c) atomic layers are about 0.25, 0.30, and 0.49 nm, respectively.

Application of Ti_3C_2X in Energy Storage. Layered materials, especially those with large interlayer spacings, are favorable intercalation hosts for the metal ions. Both theoretical calculations[25,28,38] and some experimental results[18,23,24] suggest that MXene nanosheets are promising anode materials for rechargeable Li-, Na-, K-, Mg-, Ca-, and Al-ion batteries with considerable storage capacities. Figure 5 compares the electrochemical performances of Ti_3AlC_2 and Ti_3C_2X for Li- and Na-ion storage. The raw material Ti_3AlC_2 shows a reversible capacity of 74.5 and 16.8 mAh g^{-1} for Li- and Na-ion storage (Figure 5a). Removal of the Al atoms increases the storage capacities, especially of the Na ions. Reversible capacities of about 200 and 100 mAh g^{-1} are achieved in Ti_3C_2X for Li and Na storage, respectively (Figure 5b). These improvements are attributed to the increased active storage sites and expanded interlayer spacing due to Al removal as well as the double-layer adsorption mechanism.[28] The Ti_3C_2X nanosheets exhibit excellent rate performance (Figure 5c) and long-term cycling stability (Figure 5d). Reversible storage capacities of 94.3 (for Li storage) and 53.7 (for Na storage) mAh g^{-1} can still be obtained at a current density up to 800 mA g^{-1}. After 1000 cycles at 200 mA g^{-1}, the Na-ion storage capacity maintains 68.3 mAh g^{-1}, corresponding to a decay of only 0.015% per cycle. These electrochemical performances are better than most of the Ti-based anode materials[39,40] as well as other materials such as graphite,[41] showing attractive properties for rechargeable batteries, especially for metal ions with large ionic radii, such as Na^+ and K^+.

DFT Calculated Surface Structure and Intercalation Chemistry of Ti_3C_2X. To get further insight into the surface structure and intercalation chemistry of Ti_3C_2X, DFT calculations were performed (Figure 6) using a modified model based on the above experimental results. Among the possible configurations of F and OH terminations (Supporting Information Figure S5), the one shown in Figure 6a is energetically the most

DOI: 10.1021/ja512820k
J. Am. Chem. Soc. 2015, 137, 2715–2721

favorable, where the $(OH)F_2$ or $F(OH)_2$ slabs are orderly adsorbed on the surface of the Ti_3C_2 monolayer, similar to the ordering of $LiMn_2$ in the Mn-plane of Li_2MnO_3.[42] Considering the multilayer stacking of Ti_3C_2X, its lattice parameter *c* is determined to be ca. 20.04 Å, in accordance with the above experimental results. The functional groups (e.g., OH and F) prefer to stay on the topmost sites of the Ti(c) atoms in the Ti_3C_2 monolayer. The Na ions are intercalated into the Ti_3C_2X interlayers and occupy the sites on top of the C atoms of Ti_3C_2X monolayer (Figure 6b). In addition, Al-ion intercalation leads to horizontal sliding of the Ti_3C_2X monolayer (Figure 6c). Therefore, the intercalated Al ions not only stay on top of the C atoms of one Ti_3C_2X layer but also close to the top of the Ti(s) atoms of another Ti_3C_2X layer. The detail structural difference of Ti_3C_2X and its derivatives with Na or Al intercalation can be found in Supporting Information Figure S6.

The excellent rate performance of Ti_3C_2X for Na-ion batteries is ascribed to its high electronic and ionic conductivity. Analysis illustrates that the density of states (DOS) of Ti_3C_2X is characteristic of a metallic one (Supporting Information Figure S7). The ionic conductivity is closely related to the diffusion path and barrier of Na in Ti_3C_2X. A possible spatial hopping pathway with high structural symmetry between two nearest neighboring Na adsorption sites is that the Na ions first move to the top of the nearest neighboring Ti(s) atoms (Figure 6d), and then to the top of the C atoms (Figure 6e) (top C→ top Ti(s)→ top C). The diffusion barriers for these two paths are about 0.1087 and 0.4257 eV, respectively, suggesting that it is easier to diffuse from the top C to the top Ti(s) than from the reverse direction. Furthermore, a direct pathway is designed from the top C to the other nearest top C (Figure 6f). Calculations combined with the first-principles molecular dynamics (FPMD) simulation (Supporting Information Figure S8) show that the energetically favorable diffusion pathways must be those that pass through the site on the top Ti(s). The low diffusion barrier (about 0.41 eV) indicates that it is easy for the Na ions to diffuse in Ti_3C_2X.

In comparison with the previous modeling based on Ti_3C_2X monolayer, our modeling goes a step further toward the actual situation by taking into account the multilayer stacking of Ti_3C_2X and the random adsorption of the functional groups. Therefore, our DFT calculations provide more structural information, such as the sliding of the Ti_3C_2X monolayer upon Al ion intercalation, and closer to the reality.

CONCLUSIONS

In summary, the surface structure and the intercalation mechanism of Ti_3C_2X (X = OH, F, and O) are disclosed at the atomic scale for the first time. Most of the synthesized Ti_3C_2X nanosheets incline to be multilayer-stacked and have interlayer interactions. The adsorbed functional groups (OH^-, F^-, and O^-) are randomly distributed on the surface of Ti_3C_2X and prefer to stay on the top sites of the Ti(c) atoms in the Ti_3C_2 monolayer. In addition, the Na ions can be electrochemically intercalated/deintercalated into/out of the Ti_3C_2X lattice reversibly via two-phase transition and solid-solution reaction in sequence. The intercalated Na ions prefer to occupy the top sites of the C atoms in the Ti_3C_2X monolayer. Intercalation of the Al ions leads to horizontal sliding of the Ti_3C_2X monolayer. On the basis of these experimental results, the surface model of Ti_3C_2X is modified and DFT computations are performed to further understand the physical and chemical properties of Ti_3C_2X. It shows that the Na ions can easily diffuse within Ti_3C_2X. Last but not least important, as an anode material for the Na-ion batteries, Ti_3C_2X exhibits prominent rate performance and long-term cycling stability. These findings provide information on the surface structure and the intercalation chemistry of Ti_3C_2X at the atomic level, enrich our understanding of the MXenes, and are beneficial for the material design and applications.

ASSOCIATED CONTENT

Supporting Information

Experimental and computational section; SEM images of as-received Ti_3AlC_2 (Figure S1); XRD patterns, XPS spectra (Figure S2); EDS results (Figure S3); in situ XRD patterns of Ti_3C_2X during electrochemical deintercalation of the Na-ions (Figure S4); possible configurations of Ti_3C_2X with different contents of F and OH terminations (Figure S5); the detailed structural difference of Ti_3C_2X and its derivatives with Na or Al intercalation (Figure S6); DFT calculated density of states (DOS) of Ti_3C_2X (Figure S7); first-principles molecular dynamics (FPMD) simulation of diffusion of Na ions in Ti_3C_2X (Figure S8). This material is available free of charge via the Internet at http://pubs.acs.org.

AUTHOR INFORMATION

Corresponding Authors

zxwang@iphy.ac.cn
rcyu@aphy.iphy.ac.cn

Author Contributions

Authors X.W., X.S., Y.G. contributed equally to this work.

Notes

The authors declare no competing financial interests.

ACKNOWLEDGMENTS

This work was financially supported by the National 973 Program of China (Grants Nos.2015CB251100 and 2012CB932302) and the National Natural Science Foundation of China (NSFC Nos. 51372268 and 11234013).

REFERENCES

(1) Novoselov, K. S.; Geim, A. K.; Morozov, S. V.; Jiang, D.; Zhang, Y.; Dubonos, S. V.; Grigorieva, I. V.; Firsov, A. A. *Science* **2004**, *306*, 666.
(2) Coleman, J. N.; Lotya, M.; O'Neill, A.; Bergin, S. D.; King, P. J.; Khan, U.; Young, K.; Gaucher, A.; De, S.; Smith, R. J.; Shvets, I. V.; Arora, S. K.; Stanton, G.; Kim, H. Y.; Lee, K.; Kim, G. T.; Duesberg, G. S.; Hallam, T.; Boland, J. J.; Wang, J. J.; Donegan, J. F.; Grunlan, J. C.; Moriarty, G.; Shmeliov, A.; Nicholls, R. J.; Perkins, J. M.; Grieveson, E. M.; Theuwissen, K.; McComb, D. W.; Nellist, P. D.; Nicolosi, V. *Science* **2011**, *331*, 568.
(3) Chhowalla, M.; Shin, H. S.; Eda, G.; Li, L.-J.; Loh, K. P.; Zhang, H. *Nat. Chem.* **2013**, *5*, 263.
(4) Huang, X.; Zeng, Z.; Zhang, H. *Chem. Soc. Rev.* **2013**, *42*, 1934.
(5) Novoselov, K. S. *Proc. Natl. Acad. Sci. U.S.A.* **2005**, *102*, 10451.
(6) Balendhran, S.; Walia, S.; Nili, H.; Ou, J. Z.; Zhuiykov, S.; Kaner, R. B.; Sriram, S.; Bhaskaran, M.; Kalantar-zadeh, K. *Adv. Funct. Mater.* **2013**, *23*, 3952.
(7) Song, F.; Hu, X. *Nat. Commun.* **2014**, *5*, 4477.
(8) Huang, X.; Tan, C.; Yin, Z.; Zhang, H. *Adv. Mater.* **2014**, *26*, 2185.
(9) Cao, X.; Yin, Z.; Zhang, H. *Energy Environ. Sci.* **2014**, *7*, 1850.
(10) Butler, S. Z.; Hollen, S. M.; Cao, L.; Cui, Y.; Gupta, J. A.; Gutiérrez, H. R.; Heinz, T. F.; Hong, S. S.; Huang, J.; Ismach, A. F.; Johnston-Halperin, E.; Kuno, M.; Plashnitsa, V. V.; Robinson, R. D.; Ruoff, R. S.; Salahuddin, S.; Shan, J.; Shi, L.; Spencer, M. G.; Terrones, M.; Windl, W.; Goldberger, J. E. *ACS Nano* **2013**, *7*, 2898.
(11) Xu, M.; Liang, T.; Shi, M.; Chen, H. *Chem. Rev.* **2013**, *113*, 3766.
(12) Yan, K.; Lee, H.-W.; Gao, T.; Zheng, G.; Yao, H.; Wang, H.; Lu, Z.; Zhou, Y.; Liang, Z.; Liu, Z.; Chu, S.; Cui, Y. *Nano Lett.* **2014**, *14*, 6016.

DOI: 10.1021/ja512820k
J. Am. Chem. Soc. 2015, 137, 2715−2721

(13) Wang, Q. H.; Kalantar-Zadeh, K.; Kis, A.; Coleman, J. N.; Strano, M. S. *Nat. Nanotechnol.* **2012**, *7*, 699.
(14) Tang, Q.; Zhou, Z. *Prog. Mater. Sci.* **2013**, *58*, 1244.
(15) Naguib, M.; Kurtoglu, M.; Presser, V.; Lu, J.; Niu, J. J.; Heon, M.; Hultman, L.; Gogotsi, Y.; Barsoum, M. W. *Adv. Mater.* **2011**, *23*, 4248.
(16) Barsoum, M. W.; El-Raghy, T. *Am. Sci.* **2001**, *89*, 336.
(17) Naguib, M.; Mochalin, V. N.; Barsoum, M. W.; Gogotsi, Y. *Adv. Mater.* **2014**, *26*, 992.
(18) Naguib, M.; Halim, J.; Lu, J.; Cook, K. M.; Hultman, L.; Gogotsi, Y.; Barsoum, M. W. *J. Am. Chem. Soc.* **2013**, *135*, 15966.
(19) Naguib, M.; Mashtalir, O.; Carle, J.; Presser, V.; Lu, J.; Hultman, L.; Gogotsi, Y.; Barsoum, M. W. *ACS Nano* **2012**, *6*, 1322.
(20) Ghidiu, M.; Naguib, M.; Shi, C.; Mashtalir, O.; Pan, L.; Zhang, B.; Yang, J.; Gogotsi, Y.; Billinge, S. J. L.; Barsoum, M. W. *Chem. Commun.* **2014**, *50*, 9517.
(21) Xie, X.; Chen, S.; Ding, W.; Nie, Y.; Wei, Z. *Chem. Commun.* **2013**, *49*, 10112.
(22) Lukatskaya, M. R.; Mashtalir, O.; Ren, C. E.; Dall'Agnese, Y.; Rozier, P.; Taberna, P. L.; Naguib, M.; Simon, P.; Barsoum, M. W.; Gogotsi, Y. *Science* **2013**, *341*, 1502.
(23) Naguib, M.; Come, J.; Dyatkin, B.; Presser, V.; Taberna, P.-L.; Simon, P.; Barsoum, M. W.; Gogotsi, Y. *Electrochem. Commun.* **2012**, *16*, 61.
(24) Mashtalir, O.; Naguib, M.; Mochalin, V. N.; Dall'Agnese, Y.; Heon, M.; Barsoum, M. W.; Gogotsi, Y. *Nat. Commun.* **2013**, *4*, 1716.
(25) Tang, Q.; Zhou, Z.; Shen, P. *J. Am. Chem. Soc.* **2012**, *134*, 16909.
(26) Xie, Y.; Naguib, M.; Mochalin, V. N.; Barsoum, M. W.; Gogotsi, Y.; Yu, X.; Nam, K.-W.; Yang, X.-Q.; Kolesnikov, A. I.; Kent, P. R. C. *J. Am. Chem. Soc.* **2014**, *136*, 6385.
(27) Zhao, S.; Kang, W.; Xue, J. *J. Phys. Chem. C* **2014**, *118*, 14983.
(28) Xie, Y.; Dall'Agnese, Y.; Naguib, M.; Gogotsi, Y.; Barsoum, M. W.; Zhuang, H. L.; Kent, P. R. C. *ACS Nano* **2014**, *8*, 9606.
(29) Er, D.; Li, J.; Naguib, M.; Gogotsi, Y.; Shenoy, V. B. *ACS Appl. Mater. Interfaces* **2014**, *6*, 11173.
(30) Peng, Q.; Guo, J.; Zhang, Q.; Xiang, J.; Liu, B.; Zhou, A.; Liu, R.; Tian, Y. *J. Am. Chem. Soc.* **2014**, *136*, 4113.
(31) Halim, J.; Lukatskaya, M. R.; Cook, K. M.; Lu, J.; Smith, C. R.; Näslund, L.-Å.; May, S. J.; Hultman, L.; Gogotsi, Y.; Eklund, P.; Barsoum, M. W. *Chem. Mater.* **2014**, *26*, 2374.
(32) Etacheri, V.; Marom, R.; Elazari, R.; Salitra, G.; Aurbach, D. *Energy Environ. Sci.* **2011**, *4*, 3243.
(33) Goodenough, J. B.; Kim, Y. *Chem. Mater.* **2009**, *22*, 587.
(34) Zeng, Z.; Yin, Z.; Huang, X.; Li, H.; He, Q.; Lu, G.; Boey, F.; Zhang, H. *Angew. Chem., Int. Ed.* **2011**, *50*, 11093.
(35) Zeng, Z.; Sun, T.; Zhu, J.; Huang, X.; Yin, Z.; Lu, G.; Fan, Z.; Yan, Q.; Hng, H. H.; Zhang, H. *Angew. Chem., Int. Ed.* **2012**, *51*, 9052.
(36) Pearson, D. H.; Ahn, C. C.; Fultz, B. *Phys. Rev. B* **1993**, *47*, 8471.
(37) Stoyanov, E.; Langenhorst, F.; Steinle-Neumann, G. *Am. Mineral.* **2007**, *92*, 577.
(38) Li, H.; Wu, J.; Yin, Z.; Zhang, H. *Acc. Chem. Res.* **2014**, *47*, 1067.
(39) Zhu, G.-N.; Wang, Y.-G.; Xia, Y.-Y. *Energy Environ. Sci.* **2012**, *5*, 6652.
(40) Doeff, M.; Cabana, J.; Shirpour, M. *J. Inorg. Organomet. Polym. Mater.* **2014**, *24*, 5.
(41) Cao, Y.; Xiao, L.; Ai, X.; Yang, H. *Electrochem. Solid-State Lett.* **2003**, *6*, A30.
(42) Wang, R.; He, X.; He, L.; Wang, F.; Xiao, R.; Gu, L.; Li, H.; Chen, L. *Adv. Energy Mater.* **2013**, *3*, 1358.

DOI: 10.1021/ja512820k
J. Am. Chem. Soc. 2015, 137, 2715−2721